Mon. Not. R. Astron. Soc. **354,** 621–628 (2004) doi:10.1111/j.1365-2966.2004.08223.x

# Correlation of atmospheric opacity measurements by SCUBA and an infrared radiometer

Ian M. Chapman,★ David A. Naylor and Robin R. Phillips
*Department of Physics, University of Lethbridge, 4401 University Dr., Lethbridge, Alberta, Canada, T1K 3M4*

Accepted 2004 July 13. Received 2004 July 13; in original form 2004 March 31

**ABSTRACT**

We present the results of a comparison of measured water vapour content above Mauna Kea obtained using the Submillimetre Common User Bolometer Array (SCUBA) and an infrared radiometer at the James Clerk Maxwell Telescope. We show that for most weather conditions the Infrared Radiometer for Millimetre Astronomy (IRMA) produces results that correlate well with the SCUBA measurements. However, for nights with thick cirrus cover, the IRMA results deviate from those obtained with SCUBA.

**Key words:** radiative transfer – atmospheric effects.

## 1 INTRODUCTION

Ground-based observatories operating at (sub)millimetre wavelengths are seriously hindered by the atmosphere, which absorbs, emits and scatters electromagnetic radiation. Most of the opacity in this spectral region is a result of the presence of several strongly-absorbing water vapour lines. Additional opacity arises from weaker transitions associated with molecular oxygen and ozone. To address this problem, (sub)millimetre observatories are built at dry, high-altitude sites such as Mauna Kea, Hawaii (4100 m) and Chajnantor, Chile (5000 m). Locating a (sub)millimetre observatory at a high-altitude site places it above much of the atmospheric water vapour, enabling astronomical observations in several semitransparent spectral 'windows'. Even at these high-altitude sites, however, there is still sufficient water vapour to affect observations. Furthermore, the highly polar nature of water molecules results in the non-uniform distribution of the species through the atmosphere. When this is coupled with bulk atmospheric motion above the telescope it results in rapid variations of the line-of-sight precipitable water vapour (PWV) abundance, giving rise to phase distortion of the wavefronts as they propagate through the atmosphere.

One method of correcting for wavefront phase distortion is to measure the amount of water vapour in the telescope beam. Traditionally, this has been derived through periodic skydip measurements, either with a dedicated tipping radiometer or with one of the primary telescope instruments. However, both methods have the disadvantage of yielding only an average measurement of PWV over the whole skydip rather than the desired value along the line of sight from the telescope to the source. Moreover, the former method uses an instrument that is offset from the main telescope beam, whereas the latter method requires interrupting observations to perform a skydip.

★E-mail: ian@terraengine.com

A more optimal solution is to have a device that looks along the telescope beam and directly determines the line-of-sight PWV column density without requiring skydips. For (sub)millimetre telescopes, one method has been to determine the amount water vapour from measurements of the 183-GHz water vapour line using a heterodyne receiver system. This involves measuring the intensity of three narrow bands offset by differing amounts from the line centre (which are hence sensitive to differing amounts of water vapour). This has the disadvantage of requiring a complex and difficult to maintain instrument.

We have developed an Infrared Radiometer for Millimetre Astronomy (IRMA) which employs a novel technique for measuring atmospheric water vapour content. The IRMA device is a simple infrared radiometer that observes a narrow spectral region around 20 μm (15 THz), which contains only rotational transitions of water vapour. The simplicity, and hence low cost and reliability, of such a device offers many advantages over the 183-GHz system. The ultimate goal for any water vapour monitor operating on a (sub)millimetre telescope is to provide measurements that enable water vapour induced atmospheric effects to be removed from the telescope science data. If IRMA is to be used in this capacity, the optical depth it measures at 20 μm must correlate directly with the optical depth at the operating wavelengths of the telescope (approximately 200 GHz to 1.2 THz or 1300–250 μm). In this paper we report on the results of a comparison of several months worth of IRMA data collected at the James Clerk Maxwell Telescope (JCMT) on Mauna Kea with several other sources of PWV available for this site.

## 2 ATMOSPHERIC OPACITY

The determination of the atmospheric opacity above Mauna Kea is critical for the calibration of astronomical data from the JCMT (Archibald et al. 2002). Precise measurements of the zenith sky opacity, $\tau$, must be obtained frequently to ensure proper calibration of astronomical data. This is particularly critical for the JCMT's

primary scientific instrument, the Submillimetre Common User Bolometer Array (SCUBA; Holland et al. 1999). SCUBA uses one of its pixels in a DC-biased mode to estimate the zenith sky opacity at the wavelength and azimuth of observation by performing periodic skydips. A skydip measures the emission of the atmosphere as a function of zenith angle. A radiative transfer model is then used to fit the data and determine the zenith sky opacity of the atmospheric windows used for the observation. SCUBA has been shown to provide an accurate estimate of $\tau$ provided that the weather conditions are stable and uniform across the sky (Archibald et al. 2002).

### 2.1 Radiative transfer model

In order to investigate the effect of atmospheric variations on the opacity of the windows observed by SCUBA, a radiative transfer model, known as the University of Lethbridge Transmission and Radiance Atmospheric Model (ULTRAM; Chapman 2002), was developed using the Interactive Data Language (IDL®). IDL® was chosen for this project because of its many array handling routines which allow calculations of large data sets to be performed efficiently.

Like most radiative transfer models, ULTRAM is a line-by-line, layer-by-layer model. This description refers to the method used in the calculations: the contribution to opacity of each spectral line is computed separately and summed to give the overall opacity of an atmospheric layer as a function of wavenumber. This process is repeated for each of the layers descending from the top of the atmosphere to the ground.

Several radiative transfer models have been presented in the literature. One that is used frequently is the Fast Atmospheric Signature Code (FASCODE; Chetwynd, Wang & Anderson 1994). FASCODE has been developed to be a comprehensive radiative transfer model, with the ability to simulate nearly any desired observing geometry. The program has a number of built-in atmospheric models that describe the atmosphere in general geographic locations and seasons, such as the midlatitude summer atmosphere.

While FASCODE has many strengths, it suffers from several limitations. The first is that the FASCODE atmospheric models all describe the atmosphere at general locations. To model a specific location, a user has to carefully construct and format an atmospheric model to import into FASCODE. This is a complicated process that can easily lead to errors. Another limitation is that FASCODE is immense, with the main program alone consisting of over 71 000 lines of FORTRAN code. Because of its size, FASCODE is extremely difficult to maintain and modify for specific applications.

The limitations of FASCODE provided the impetus for the development of ULTRAM, whose goal was to simplify the generation of space-to-ground, location-specific atmospheric models. ULTRAM exploits the graphical user interface (GUI) and visualization capabilities of IDL. Users can easily create and import atmospheric models through the use of a GUI or text files. A model of the atmosphere above Mauna Kea has been created using atmospheric parameters derived by averaging numerous radiosondes launched from nearby Hilo airport. This results in a more accurate spectrum for Mauna Kea than would be produced by the tropical atmosphere profile contained in FASCODE.

Although ULTRAM does not have the complex geometrical capabilities of FASCODE, it is a compact program designed to model atmospheric transmission for the astronomical community. Consisting of $\sim$1000 lines of a modern programming language, IDL®, ULTRAM is significantly more user-friendly and maintainable than other radiative transfer models. We have used ULTRAM extensively to generate the theoretical spectra presented in this paper.

A paper describing ULTRAM is currently in preparation. It is our intention that ULTRAM be made freely available to the scientific community using the free IDL® Virtual Machine Licence once development of a GUI is complete. Further information on ULTRAM can be obtained by contacting the authors.

### 2.2 Modelling the atmosphere above Mauna Kea

Under good observing conditions, the atmosphere above Mauna Kea has several (sub)millimetre windows, spectral regions where the atmosphere is semitransparent. Two of these windows, centred on 850 and 450 μm, and shown in Figs 1 and 2 respectively, are those

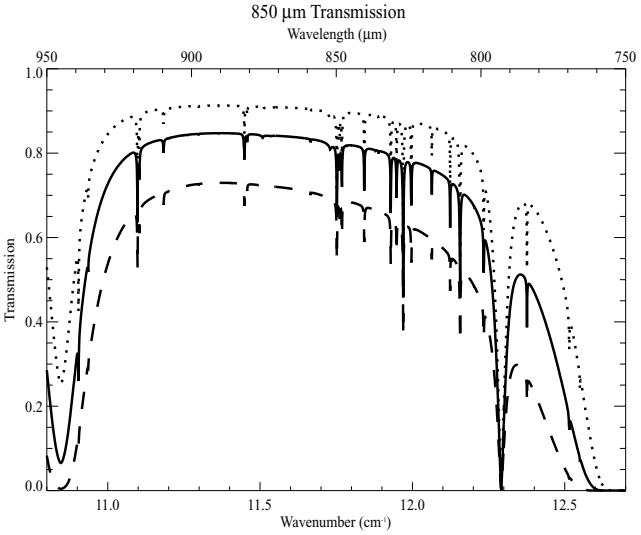


**Figure 1.** The transmission of the 850-μm window for the atmosphere above Mauna Kea with water vapour column abundances of 0.5 (dotted line), 1.0 (solid line) and 2.0 (dashed line) mm PWV as modelled using ULTRAM.

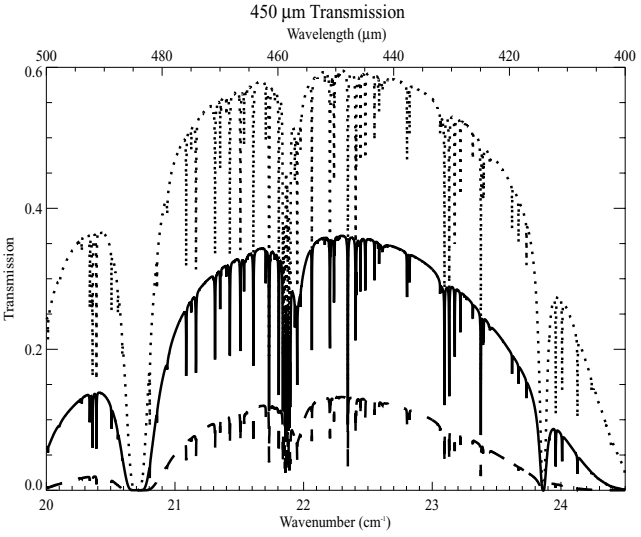


**Figure 2.** The transmission of the 450-μm window for the atmosphere above Mauna Kea with water vapour column abundances of 0.5 (dotted line), 1.0 (solid line) and 2.0 (dashed line) mm PWV as modelled using ULTRAM.

observed by SCUBA to determine atmospheric opacity. The main contributors to opacity in these spectral regions are water vapour, molecular oxygen and ozone. The strongest transitions are those due to water vapour; because water vapour exists mainly in the lower atmosphere, these transitions are dominated by pressure broadening, resulting in a modified Voigt line shape (Clough, Kneizys & Davies 1989). Ozone produces a manifold of weak, narrow lines. Because, in the tropics, the highest concentrations of ozone are found at an altitude of ∼25 km, the ozone line shape is dominated by thermal effects, resulting in a Doppler (Gaussian) profile.

The intensity of the radiation exiting the bottom of the atmosphere, $I$, in W m$^{-2}$ sr$^{-1}$ Hz$^{-1}$ is related to the intensity of radiation entering the atmosphere from space, $I_0$, by the radiative transfer equation:

$$I = I_0\left\{\exp\left[-\int_{z_0}^{l} k_\sigma n(z)\,\mathrm{d}z\right]\right\} + B(\sigma, T)\left\{1-\exp\left[-\int_{z_0}^{l} k_\sigma n(z)\,\mathrm{d}z\right]\right\}. \quad (1)$$

Here, $n(z)$ is the number density of the absorbing species at altitude $z$, $z_0$ is the altitude of observation, $l$ is the altitude of the top of the atmosphere, $k_\sigma$ is the absorption coefficient of the atmosphere at wavenumber, $\sigma$, and $B(\sigma, T)$ is the Planck blackbody function at $\sigma$ and temperature, $T$. Because $\tau$ is defined as $\int_{z_0}^{l} k_\sigma n(z)\,\mathrm{d}z$, equation (1) can be written as

$$I = I_0[\exp(-\tau)] + B(\sigma, T)[1-\exp(-\tau)]. \quad (2)$$

In practice, equation (2) is modified to include radiative effects due to emission from components in the optical train of the telescope, $J_{\mathrm{tel}}$. For example, for the JCMT this would include emission from the membrane and the warm telescope optics. The modified radiative transfer equation can be written as

$$I = I_0[\exp(-\tau)] + B(\sigma, T)[1-\exp(-\tau)] + J_{\mathrm{tel}}. \quad (3)$$

The first term in equation (3) describes the absorption of radiation that originates from space. SCUBA skydips assume that no bright astronomical sources are sampled, so the only radiation from space is a result of the cosmic microwave background (CMB). Emissions from the atmosphere sufficiently dominate the CMB in these wavelengths, so the absorption term can be neglected in equation (3), leaving

$$I = B(\sigma, T)[1-\exp(-\tau)] + J_{\mathrm{tel}}. \quad (4)$$

Under the assumption of a plane-parallel atmosphere and integrating over the spectral band, equation (4) can be expressed in terms of the zenith angle, $\theta$, or equivalently airmass, $A$, defined as sec$\theta$. Equation (4) becomes

$$I = \int_{\mathrm{band}} [B(\sigma, T)[1-\exp(-\tau)] + J_{\mathrm{tel}}]\,\mathrm{d}\sigma. \quad (5)$$

Data from the measured skydips are fitted to this equation to produce $\tau$-values.

While SCUBA determines $\tau$ by fitting an atmospheric model to the skydips it obtains, ULTRAM has been used to determine theoretical $\tau$-values through direct calculations. An opacity cube has been produced by using ULTRAM to model the atmosphere above Mauna Kea for the wavenumber range of 5–50 cm$^{-1}$ (2000–200 μm) as a function of water vapour column abundance (0–2 mm PWV in steps of 0.1 mm PWV). Base conditions for the atmospheric model were determined by averaging data from radiosondes, which are launched twice daily (0:00 and 12:00 UT) from Hilo airport, approximately 40 km from Mauna Kea. Data from 80 radiosondes launched in the evenings (12:00 UT) between 2000 June and October, downloaded from http://weather.uwyo.edu/upperair/sounding.html, have been averaged; the results are shown in Table 1. Table 1 also shows the column amounts of the molecules used in the Mauna Kea simulations, which were determined using molecular mixing ratios taken from the tropical atmosphere profile in FASCODE3 (Chetwynd et al. 1994). The temperature and pressure profiles for the lower atmosphere (4.092–12 km) were determined from the base conditions in Table 1, while those in the upper atmosphere (above 12 km) were taken from the FASCODE3 tropical atmosphere profile. The modelled Mauna Kea pressure–temperature curve is shown in Fig. 3. The 850- and 450-μm spectral bands are defined by the filter profiles of SCUBA (Naylor & Holland 2001).

**Table 1.** Input parameters for ULTRAM atmospheric model of the summit of Mauna Kea.

| | |
|---|---|
| Base pressure | 625 mBar |
| Base temperature | 273 K |
| Lapse rate | −5.6 K km$^{-1}$ |
| Scaleheight | 2 km |
| $H_2O$ column amount | $3.346 \times 10^{21}$ cm$^{-2}$ (1 mm PWV) |
| $CO_2$ column amount | $4.395 \times 10^{21}$ cm$^{-2}$ |
| $O_3$ column amount | $7.497 \times 10^{18}$ cm$^{-2}$ |
| $N_2O$ column amount | $3.964 \times 10^{18}$ cm$^{-2}$ |
| CO column amount | $1.189 \times 10^{18}$ cm$^{-2}$ |
| $CH_4$ column amount | $2.146 \times 10^{19}$ cm$^{-2}$ |
| $O_2$ column amount | $2.784 \times 10^{24}$ cm$^{-2}$ |

A theoretical $\tau$-value has been determined for each water vapour column abundance in the data cube by averaging the modelled opacity over each of the 850- and 450-μm spectral bands. Equation (5) shows that the value of $\tau$ varies linearly with airmass (or, equivalently, water vapour column abundance), so linear regression was used to determine a relation between the two quantities. For the 850-μm window, the column abundance of water vapour can be expressed as a function of opacity

$$PWV = 4.10\tau_{\mathrm{SCUBA850}} - 0.36. \quad (6)$$

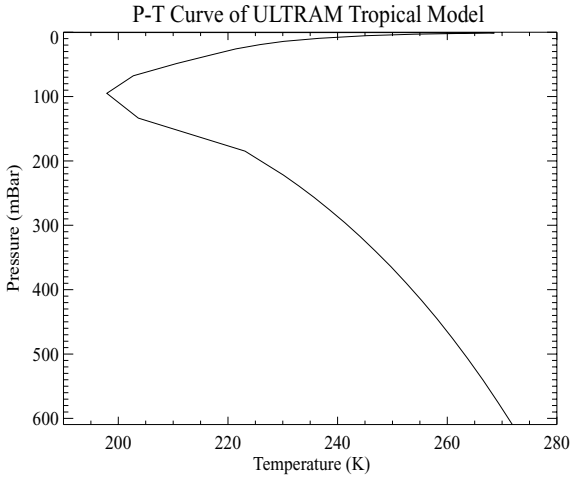


**Figure 3.** The pressure–temperature curve from the ULTRAM atmospheric model for Mauna Kea.

The corresponding relation for the 450-μm window is

$$PWV = 0.83\tau_{\mathrm{SCUBA450}} - 0.04. \quad (7)$$

Relations between $\tau_{\mathrm{SCUBA850}}$ and $\tau_{\mathrm{CSO225}}$, and $\tau_{\mathrm{SCUBA450}}$ and $\tau_{\mathrm{CSO225}}$ have been experimentally determined (Archibald et al. 2002) to be

$$\tau_{\mathrm{SCUBA850}} = 4.02\tau_{\mathrm{CSO225}} - 0.004 \quad (8)$$

and

$$\tau_{\mathrm{SCUBA450}} = 26.2\tau_{\mathrm{CSO225}} - 0.37, \quad (9)$$

respectively.

A relation between water vapour column amount and $\tau_{\mathrm{CSO225}}$ (Davis et al. 1997) has been determined to be

$$PWV = 20\tau_{\mathrm{CSO225}} - 0.32. \quad (10)$$

Combining equation (10) with equations (8) and (9) and rearranging for PWV yields

$$PWV = 5.0\tau_{\mathrm{SCUBA850}} - 0.30 \quad (11)$$

and

$$PWV = 0.76\tau_{\mathrm{SCUBA450}} - 0.04. \quad (12)$$

We believe that the theoretical relations in equations (6) and (7) are more accurate than the relations we have derived from the SCUBA/Caltech Submillimetre Observatory (CSO) $\tau$ relations (Archibald et al. 2002) because the data cube produced by ULTRAM was based on radiosonde data from the atmosphere above Mauna Kea. By comparison, equations (11) and (12) are derived from equations (8) and (9), respectively, which make use of the US Standard Atmosphere 1976 (Hazell 1991), which is not representative of the atmosphere above Mauna Kea.

## 3 IRMA CONCEPT

Measurements of atmospheric opacity above Mauna Kea in the 20-μm atmospheric window, using a high-resolution infrared Fourier transform spectrometer, have shown that over a large part of this region the atmospheric absorption, and hence emission, is dominated by pure rotational transitions of water vapour (Naylor et al. 1984). Detailed modelling shows that it is possible to select a continuous region containing several hundred water vapour lines, the vast majority of which are unsaturated for column abundances of $\leqslant$1 mm PWV above Mauna Kea. At lower altitude sites, the lines in this spectral region become saturated and thus the technique becomes less sensitive.

An infrared approach to water vapour measurement is attractive for several reasons. First, because the wavelength of 20 μm lies near the peak of the Planck curve for typical atmospheric temperatures, the spectral radiance from atmospheric water vapour at infrared wavelengths is $\sim$ three orders of magnitude greater than at radio frequencies. Secondly, the infrared radiometer uses a spectral bandwidth $\sim$ three orders of magnitude greater than the radio frequency technique. The resulting increase in flux can be traded in terms of more sensitive measurements, faster operation, smaller instrument size, or some combination thereof. Thirdly, infrared photoconductive detectors offer high operating speeds, stability and simple electronics. Finally, being a passive device (specifically, not containing a local oscillator), an infrared radiometer can be placed in close proximity to sensitive radio frequency instrumentation without risk of interference.

A prototype infrared radiometer for the measurement of atmospheric water vapour (IRMA I) was developed and tested at the JCMT in 1999 December (Smith, Naylor & Feldman 2001). The radiometer consisted of a liquid-nitrogen-cooled mercury–cadmium–telluride (MCT) photoconductive detector that alternately viewed the atmosphere, and ambient and liquid nitrogen blackbody references. This was accomplished by means of a stationary parabolic mirror and a scanning plane mirror. The scanning mirror provided a range of observable zenith angles from 0 to 70.38° in steps of 0.18°, corresponding to an airmass range from 1 to 3. The optical input to the detector was chopped at 200 Hz by a reflective chopper blade so that the detector was alternately presented with views of the atmosphere (or the blackbodies) and a reflected view of its own cold environment. The modulated detector signal was amplified, synchronously detected by means of a lock-in amplifier, digitized by a 12-bit analogue-to-digital converter (ADC) and the resulting data were logged to a file.

The radiometer was primarily operated in continuous scan mode in which the atmospheric emission was measured as a function of airmass, these data being referred to as skydips (a skydip of 1–3 airmass taking $\sim$30 s). IRMA can also be operated in stare mode, pointing along the line of sight of astronomical observations. In this mode, IRMA makes observations at a rate of 10 Hz, periodically performing skydips ($\sim$1 per hour) for calibration.

Analysis of the IRMA I skydips has shown that the infrared technique holds much promise for the challenging requirements of phase correction of the next generation of (sub)millimetre interferometers. Key elements of the prototype radiometer have subsequently been improved, and include a more sensitive MCT photoconductive detector, a resonant grid long-pass filter (Lee, Ade & Haynes 1996) (this technology is well established at submillimetre and far-infrared wavelengths but has only recently been extended to shorter wavelengths), a custom lock-in amplifier and a high-resolution (24-bit) $\Delta\Sigma$ ADC, which is synchronously triggered by a notch on the reflecting chopper wheel.

Finally, the IRMA software was modified to allow for remote operation. In this paper we present results obtained with IRMA operating on the apron of the JCMT between 2000 December and 2001 March.

## 4 ANALYSIS METHOD

### 4.1 Curve-of-growth

Between 2000 December and 2001 March, IRMA was set up to collect a series of skydips simultaneously with SCUBA skydips. A total of 1893 IRMA skydips were obtained during this period. Because of IRMA's location outside the JCMT membrane, it did not share exactly the same azimuthal angle as the telescope because of small offsets between the carousel and telescope. However, the alignment was sufficiently close that we expected the IRMA and SCUBA skydips would be correlated. The number of IRMA skydips for which corresponding SCUBA skydips exist is 613. The data were then filtered based on the quality of the skydips. Low-quality skydips, caused by factors such as cryogen depletion or scanning past atmospheric cloud banks, were identified by either high or low voltages, or by poor fit with an exponential curve (i.e. wavy skydips). These flagged skydips were removed from the data set, leaving 533, or $\sim$87 per cent, of the time-matched subset (see Table 2).

As a part of the skydip cycle, IRMA obtained several calibration measurements of hot and cold loads, allowing a determination of the

**Table 2.** A summary of the IRMA skydips collected over the period from 2000 December to 2001 March.

| | |
|---|---|
| Total number of IRMA skydips | 1893 |
| Number time-matched with SCUBA | 613 |
| Number rejected for poor quality | 80 |
| Number used in comparison with SCUBA | 533 |
| Number used in comparison with CSO | 1278 |

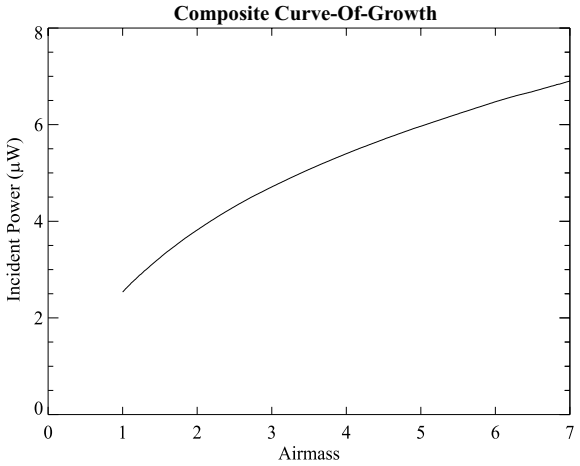


**Figure 4.** The mean, composite curve-of-growth determined from individual IRMA skydips which forms the basis for establishing $\tau_{\rm IRMA}$ in equation (14) for comparison with $\tau_{\rm SCUBA850}$, $\tau_{\rm SCUBA450}$ and $\tau_{\rm CSO225}$. In this figure, the incident power at an airmass of 1 corresponds to a water vapour column abundance of 0.5 mm PWV (Chapman 2002).

instrumental responsivity, $R_{\rm inst}$ ($VW^{-1}$), which relates the incident power on the radiometer, $\Phi$ ($W$), to the voltage measured, $V$, by

$$\Phi = \frac{V}{R_{\rm inst}}. \tag{13}$$

Using this equation, the skydips were calibrated to give incident power as a function of airmass.

Once calibrated, the data can be used to generate a curve-of-growth (Houghton 1986), as in Fig. 4, which shows the spectrally integrated emission of an absorbing species as the abundance of the species is varied. In the case of the atmosphere, the abundance of water vapour is varied by the process of performing a skydip, observing the sky at increasing zenith angles or, equivalently, airmass. To simplify the analysis, it is assumed that the vertical pressure and temperature profiles and water vapour scaleheight do not vary significantly from day to day. Analysis of 80 pressure–temperature curves from radiosondes, launched from nearby Hilo airport, supports this assumption.

Under these assumptions, it is possible to construct a curve-of-growth by rescaling, or stretching, the horizontal axes of the individual skydips to reflect the water vapour amount at the times of observation. Fig. 5 shows two IRMA skydips in the upper-left panel. The higher skydip was collected at a time of higher water vapour content than the lower. Stretching is accomplished by using a fitting routine to find a stretch factor, $F$, where the difference of the overlapping region between the top and the bottom skydips is minimized. This step is shown in the upper-right panel of Fig. 5. The top skydip is stretched, by the fitting program, to fit the lower skydip until an optimal stretch factor is found. The upper skydip is

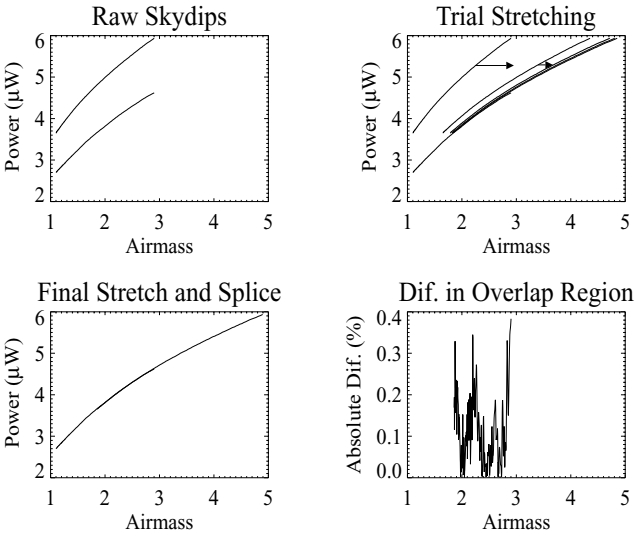


**Figure 5.** Sample output from the stretch-and-splice routine used in the analysis of IRMA data. The upper skydip in the top-left panel was collected during a time of higher atmospheric water vapour content than the lower skydip. In the top-right panel, the fitting routine guesses several stretch factors before finding the optimal value, which is shown in the bottom-left panel. The bottom-right panel shows the absolute difference between the skydips in the final overlapping area.

in its optimal position in the bottom-left panel of the figure, with the absolute per cent difference between the overlapping sections of the skydips shown in the bottom-right panel. The upper skydip is then spliced to the lower by averaging the overlapping regions of the two skydips. This process is termed stretch-and-splice.

Using the stretch-and-splice method, a basis curve-of-growth is constructed from five IRMA skydips chosen to cover the entire vertical range of the data set. A mean, composite curve-of-growth is generated from all of the skydips by stretch-and-splicing each to the basis curve-of-growth. A base opacity for the IRMA 20-μm spectral region, or $\tau_{\rm IRMA}$, is determined by fitting the mean, composite curve-of-growth to an exponential function and taking the value of the exponent as $\tau^*_{\rm IRMA}$. The IRMA skydips are then fitted to the mean, composite curve-of-growth using the stretch-and-splice method, and the stretch factors, $F$, from the fitting routine are used to determine a $\tau_{\rm IRMA}$ for the individual skydips using the simple relation

$$\tau_{\rm IRMA} = \tau^*_{\rm IRMA} F. \tag{14}$$

These resulting IRMA opacities can then be compared to the corresponding time-matched SCUBA opacities.

## 5 RESULTS

### 5.1 SCUBA 850-μm

Fig. 6 shows $\tau_{\rm IRMA}$ plotted against $\tau_{\rm SCUBA850}$. In this figure, each circle represents the $\tau$ value calculated for a single IRMA skydip. Circles appear in vertical groups because several IRMA skydips can be performed during a single SCUBA skydip. The appearance of columnar grouping in the data indicates that the atmospheric water vapour content changes appreciably during the time that SCUBA performs a skydip (∼7 m). The linear least-squares fit to the data is also shown. Most of the data points are tightly clustered about the

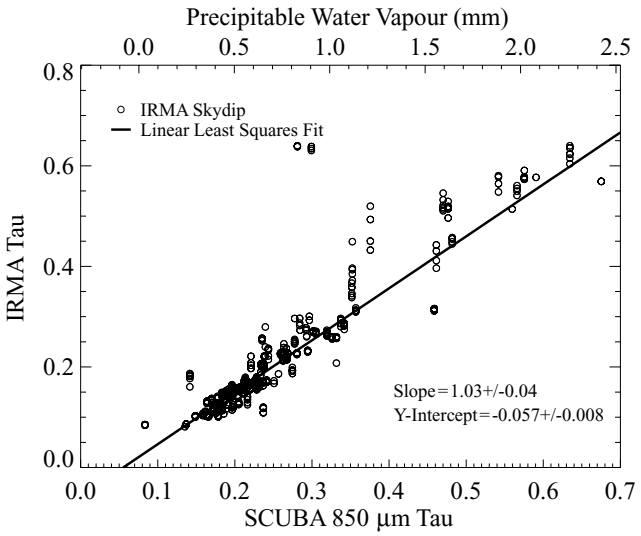


**Figure 6.** Comparison of IRMA and SCUBA 850-μm atmospheric opacity measurements.

line, indicating a high degree of correlation between the measurements, as expected. The correlation coefficient for these data is $r^2 = 0.924$. The slope of the line shows that the 850-μm spectral region saturates slightly faster than the infrared region observed by IRMA. The non-zero intercept of the line indicates that water vapour is not the only species responsible for atmospheric opacity in the 850-μm band. Atmospheric modelling (see Fig. 1) shows that this non-zero intercept is to be expected because the 850 μm region contains numerous ozone and oxygen lines that provide an additional source of opacity not present at 20 μm. The top scale in Fig. 6, calculated from equation (6), shows that the $x$-intercept of the least-squares fit falls close to 0 mm PWV, indicating that IRMA is only sensitive to atmospheric water vapour.

### 5.2 SCUBA 450-μm

Fig. 7 shows $\tau_{\mathrm{IRMA}}$ plotted against $\tau_{\mathrm{SCUBA450}}$. As in Fig. 6, each circle represents the $\tau$ value calculated for an IRMA skydip. Circles again appear in vertical groups because the atmospheric water vapour content changes appreciably during a single SCUBA skydip. The linear least-squares fit to the data is shown, and again a high degree of correlation (correlation coefficient, $r^2 = 0.867$) is indicated by the tight clustering of circles about the line. The slope of the line shows that the 450-μm spectral region saturates much faster than the infrared region observed by IRMA. The small, non-zero intercept of the line indicates that water vapour is the main species responsible for atmospheric opacity in the 450-μm region with a small amount of opacity due to numerous ozone lines (see Fig. 2). However, this additional opacity due to the stratospheric ozone lines in the 450-μm region is less significant because the opacity due to tropospheric water vapour is much higher in this region. The top scale in Fig. 7, calculated from equation (7), again shows that IRMA only measures opacity due to atmospheric water vapour.

### 5.3 CSO 225-GHz tau

The CSO (Phillips 1990) operates a 225-GHz skydipper that for many years has been the primary source of opacity measurements for the (sub)millimetre telescopes on Mauna Kea. It was operating for most of the IRMA run, returning an opacity value every 10 m, thereby yielding a large data set against which the IRMA skydips can be compared. However, the CSO skydips have a reputation of being unreliable around sunrise and sunset and can also have large errors in weather that changes rapidly (because the skydip is an average of the whole sky in the direction that the dipper is pointing). To minimize these problems, the JCMT produces a 'CSO fits' archive (online at http://www.jach.hawaii.edu/JAClocal/JCMT/jcmt_tau.html), which is a subset of all CSO skydips that have been filtered to include only those points that have a nearby SCUBA skydip that returned a similar value. A smooth polynomial is then fitted to these data points, which can then be used to give a CSO value for any time for which a fit is available. Fig. 8 shows all of the continuous IRMA skydips (1278) for which there was an available CSO fit. This produces a considerably better fit than the equivalent figure with the unfiltered CSO data points. The correlation coefficient for these data is $r^2 = 0.716$. Equation (10) is used to produce the top scale in Fig. 8, which relates $\tau_{\mathrm{CSO225}}$ to atmospheric water vapour content.

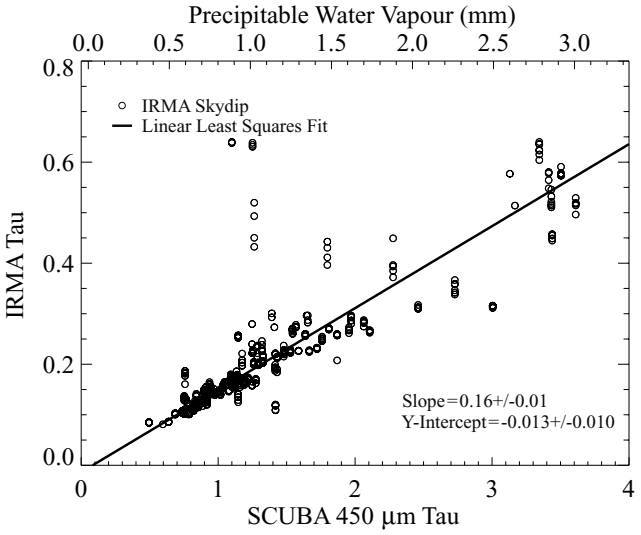


**Figure 7.** Comparison of IRMA and SCUBA 450-μm atmospheric opacity measurements.

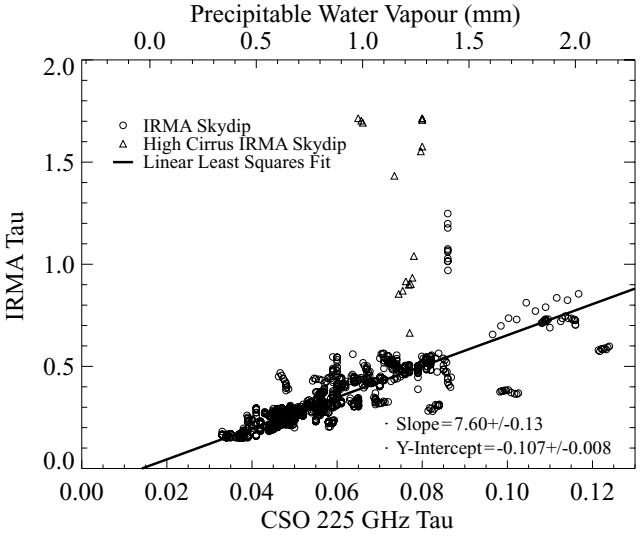


**Figure 8.** Comparison of IRMA and CSO 225-GHz atmospheric opacity measurements.

One of the main concerns with the IRMA concept is that the opacity in the 20-μm wavelength range is affected by the presence of cirrus clouds which have little impact at wavelengths of 1 mm. Unfortunately, during the IRMA campaign at the JCMT we did not have a method in place for tracking the amount of cirrus on any given night. We are not aware of any automated systems (e.g. all-sky cameras) that were operating on Mauna Kea in 2000. However, the United Kingdom Infrared Telescope (UKIRT) operators keep a written log of the weather conditions with an estimate of the cirrus cover on a scale of 1:8. We obtained this log and checked for nights during the IRMA campaign where the estimate was 7/8 or 8/8 of cirrus cover. For the 40-d IRMA campaign there was only one night where this level of cirrus cover was recorded; the corresponding points are plotted as triangles in Fig. 8. The log notes that on this night the cirrus was sufficiently thick that the UKIRT was unable to operate.

It can be clearly seen that in the extreme case (which occurred once in the 40-d period) IRMA does generate incorrect readings. The remaining vertical column of points and the three groupings of points well below the best-fitting line both come from the last couple of days of operation in March, just before the instrument failed – possibly implying some other problem with these data. However, the rest of the data, taken over the time period from mid-December to early February, are a remarkably good fit especially considering that the CSO $\tau$-meter points in a fixed azimuth position, which is generally different than the JCMT. The correlation coefficient of the data in Fig. 8 is $r^2 = 0.844$ if the cirrus is not included, nearly as high as the correlation of $\tau_{\rm IRMA}$ with $\tau_{\rm SCUBA850}$.

Further analysis to determine a relationship between the number of 'eighths' entered in the UKIRT log and the distance from the line of best fit for points on a given night showed no detectable trend.

We draw two conclusions from this (data limited) analysis of cirrus effects: (i) small amounts of cirrus, as is fairly common on Mauna Kea, have no detectable effect on the IRMA data; (ii) nights where the cirrus is thick enough to be problematic at infrared wavelengths are uncommon.

Future IRMA campaigns will attempt to address this issue further. We note that a potential solution would be to add a second infrared detector channel, specifically tuned to measure cirrus emission, which could then be removed in post-processing.

## 6 CONCLUSIONS

Measurements of the column abundance of atmospheric water vapour above Mauna Kea obtained with an infrared radiometer show a high degree of correlation with other measures of water vapour available on the summit of Mauna Kea. Correlation coefficients for each of the SCUBA and CSO comparisons are shown in Table 3.

The line of best fit through the comparison data shows that, on nights when IRMA is unaffected by cirrus clouds, IRMA measures exclusively water vapour emission while some of the opacity in the bands observed by SCUBA is a result of other species. Relations between $\tau_{\rm IRMA}$ and opacity measurements from the comparison instruments are given in Table 4. This is evidenced by the non-zero $x$-intercepts of the linear least-squares fits in the figures that correspond to water vapour column abundances of 0 mm PWV. Atmospheric modelling shows that this additional opacity is a result of molecular oxygen and ozone.

**Table 3.** A summary of the correlation coefficients for the $\tau_{\rm IRMA}$ comparisons.

| Comparison instrument | Correlation coefficient |
|---|---|
| SCUBA 850-μm | 0.924 |
| SCUBA 450-μm | 0.867 |
| CSO 225-GHz (cirrus included) | 0.716 |
| CSO 225-GHz (cirrus excluded) | 0.844 |

**Table 4.** A summary of the relations between $\tau_{\rm IRMA}$ and opacity measurements from the comparison instruments (SCUBA and CSO).

| Comparison instrument | Tau relation |
|---|---|
| SCUBA 850-μm | $\tau_{\rm IRMA} = 1.03\,\tau_{\rm SCUBA850} - 0.057$ |
| SCUBA 450-μm | $\tau_{\rm IRMA} = 0.16\,\tau_{\rm SCUBA450} - 0.013$ |
| CSO 225-GHz | $\tau_{\rm IRMA} = 7.60\,\tau_{\rm CSO225} - 0.107$ |

IRMA measurements of atmospheric opacity also show a correlation with corresponding measurements made by the 225-GHz skydipper (see Fig. 8). Although these data sets are less well correlated, this is not unexpected because the CSO $\tau$-meter is located on a different part of Mauna Kea and operates at a fixed azimuth. Even so, the linear least-squares fit to the data again intersects the $x$-axis at a $\tau$-value corresponding to a water vapour column abundance of 0 mm PWV, indicating that IRMA is sensitive to water vapour alone.

A third, improved version of IRMA will soon be completed and tested in 2004 June at Mauna Kea. These new IRMA devices are more self-contained than the previous versions and are designed to operate for long periods of time requiring no maintenance. The goal of the site tests is to prove that IRMA is a powerful water vapour detector for use in phase-delay compensation for radio telescope arrays.

## ACKNOWLEDGMENTS

We wish to thank the following individuals: Graeme Smith for his work on the IRMA prototype and for his assistance in the data analysis; Professor Ian Robson and the JCMT staff for making their facilities available for our use and for their assistance in the operation and maintenance of IRMA; Greg Tompkins for outstanding electronics support; and Brad Gom for his assistance with the data analysis. This work has made use of data from the $\tau$ archive maintained by the California Submillimetre Observatory. The JCMT is operated by the Joint Astronomy Centre on behalf of the UK Particle Physics and Astronomy Research Council, the Netherlands Organization for Pure Research and the National Research Council of Canada.

## REFERENCES

Archibald E. N. et al., 2002, MNRAS, 336, 1
Chapman I. M., 2002, MSc thesis, Univ. Lethbridge
Chetwynd J. H., Wang J., Anderson G. P., 1994, in J. Wang, P. B. Hays, eds, Proc. SPIE Vol. 2266, Optical Spectroscopic Techniques and Instrumentation for Atmospheric and Space Research. SPIE, Bellingham, p. 613
Clough S. A., Kneizys F. X., Davies R., 1989, Atmospheric Research, 23
Davis G. R., Naylor D. A., Griffin M. J., Clark T. A., Holland W. S., 1997, Icarus, 130
Hazell A. S., 1991, PhD thesis, Univ. London
Holland W. S. et al., 1999, MNRAS, 303, 659
Houghton J. T., 1986, The Physics of Atmospheres. Cambridge University Press, Cambridge

Lee C., Ade P. A. R., Haynes C. V., 1996, in ESA SP-388, Proc. 30th ESLAB Symp., Submillimetre and Far-Infrared Space Instrumentation. ESTEC, Noordwijk, p. 81

Naylor D. A., Holland W. S., 2001, Technical report, Measuring the SCUBA Wideband Filters Using the University of Lethbridge FTS. JCMT

Naylor D. A., Boreiko R. T., Clark T. A., Emery R. J., Fitton B., Kessler M. F., 1984, PASP, 96, 167

Phillips T. G., 1990, From Ground-Based to Space-Borne Sub-mm Astronomy. Caltech Submillimeter Observatory

Smith G. J., Naylor D. A., Feldman P. A., 2001, Int. J. Infrared Millim. Waves, 22, 661

This paper has been typeset from a TEX/LATEX file prepared by the author.